in: Advances in Atomic and Molecular Physics

ed.: B. Bederson and H. Walther, 2002

Multiple Ionization in Strong Laser Fields

R. Dörner*[1], Th. Weber[1], M. Weckenbrock[1], A. Staudte[1],

M. Hattass[1], R. Moshammer[2], J. Ullrich[2], H. Schmidt-Böcking[1]

[1]*Institut für Kernphysik, August Euler Str.6, 60486 Frankfurt, Germany*

[2]*Max-Planck-Institut für Kernphysik,*

*Saupfercheckweg 1, 69117 Heidelberg, Germany**

(Dated: 24.9.2001)

*Electronic address: E-mail:doerner@hsb.uni-frankfurt.de

CONTENTS

I. INTRODUCTION

70 years ago Maria Göppert-Mayer [1] showed that the energy of many photons can be combined to achieve ionization in cases where the energy of one photon is not sufficient to overcome the binding. Modern short pulse Ti:Sa lasers ($800nm, 1.5eV$) routinely provide intensities of more than $10^{16}W/cm^2$ and pulses shorter than 100 femtoseconds. Under these conditions the ionization probability of most atoms is close to unity. $10^{16}W/cm^2$ corresponds

to about 10^{10} coherent photons in a box of the size of the wavelength ($800nm$). This extreme photon density allows highly nonlinear multiphoton processes such as multiple ionization, where typically more than 50 photons can be absorbed from the laser field.

Such densities of coherent photons in the laser pulse also suggests a change from the "photon-" to the "field-perspective" : The laser field can be described as a classical electromagnetic field, neglecting the quantum nature of the photons. From this point of view the relevant quantities are the field strength and its frequency. $10^{16}W/cm^2$ at $800nm$ corresponds to a field of $3 \cdot 10^{11}V/m$ comparable to the field experienced by the electron on a Bohr orbit in atomic hydrogen ($5 \cdot 10^{11}V/m$).

Single ionization in such strong fields has been intensively studied for many years now. The experimental observables are the ionization rates as function of the laser intensity and wavelength, the electron energy and angular distribution as well as the emission of higher harmonic light. We refer the reader to several review articles covering this broad field [2–4]. Also the generation of femtosecond laser pulses has been described in a number of detailed reviews [5–8].

The present article focuses on some recent advances in unveiling the mechanism of *double and multiple ionization* in strong fields. Since more particles are involved, the number of observables and the challenge to the experimental as well as to the theoretical techniques increases. Early studies measured the rate of multiply charged ions as a function of laser intensity. The work reviewed here employs mainly COLTRIMS (Cold Target Recoil Ion Momentum Spectroscopy) [9] to detect not only the charge state but also the momentum vector of the ion and of one of the electrons in coincidence. Today such highly differential measurements are standard in the fields of ion-atom, electron-atom and high energy single photon-atom collision studies.

The main question discussed in the context of strong fields as well as in the above mentioned areas of current research is the role of electron correlation in the multiple ionization process. Do the electrons escape from the atom "sequentially" or "nonsequentially", i.e. does each electron absorb the photons independently, or does one electron absorb the energy from the field and then share it with the second electron via electron-electron correlation?

Despite its long history the underlying question of the dynamics of electron correlation is still one of the fundamental puzzles in quantum physics. Its importance lies not only in the intellectual challenge of the few-body problem, but also in its wide ranging impact

to many fields of science and technology. It is the correlated motion of electrons, which is responsible for the structure and the evolution of large parts of our macroscopic world. It drives chemical reactions, is the ultimate reason for superconductivity and many other effects in the condensed phase. In atomic processes few-body correlation effects can be studied in a particular clear manner. This, for example, was the motivation for studying theoretically and experimentally the question of double ionization by charged particle (see [10] for a review) or single photon [11, 12] impact in great detail. As soon as lasers became strong enough to eject two or more electrons from an atom, electron correlation in strong light fields became subject of increased attention, too. As we will show below, in comparison with some of the latest results on double ionization by ion and single photon impact, the laser field generates new correlation mechanisms thereby raising more exciting new questions than settling old ones.

II. COLTRIMS – A CLOUD CHAMBER FOR ATOMIC PHYSICS

For a long time the experimental study of electron correlation in ionization processes of atoms, molecules and solids has suffered from the technical challenge to observe more than one electron emerging from a multiple ionization event. The main problem lies in performing coincidence studies employing conventional electron spectrometers, which usually cover only a small part of the total solid angle. COLTRIMS (Cold Target Recoil Ion Momentum Spectroscopy) is an imaging technique, which solves this fundamental problem in atomic and molecular coincidence experiments. Like the cloud chamber and its modern successors in nuclear and high energy physics, it delivers complete images of the momentum vectors of all charged fragments from an atomic or molecular fragmentation process. The key feature of this technique is to provide a 4π collection solid angle for low energy electrons (up to a few hundred eV) in combination with 4π solid angle and high resolution for the coincident imaging of the ion momenta.

As we will show below the ion momenta in most atomic reactions with photons or charged particles are of the same order of magnitude as the electron momenta. Due to their mass, however, this corresponds to ion energies in the range of μeV to meV. These energies are below thermal motion at room temperature. Thus, the atoms have to be substantially cooled before the reaction. In the experiments discussed here this is achieved by using a supersonic

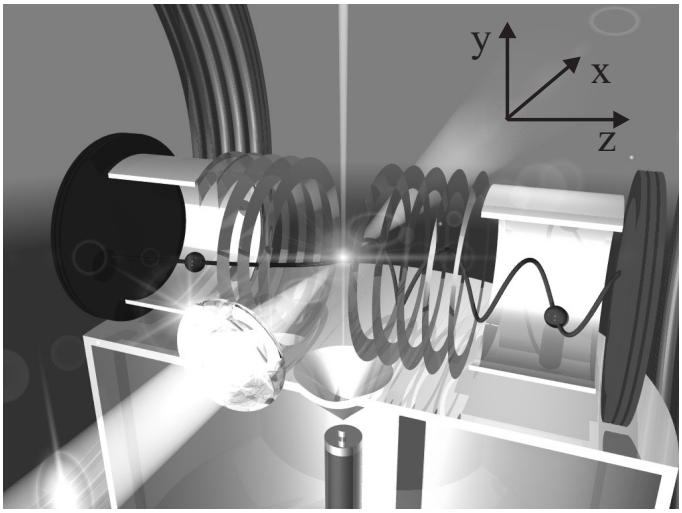

FIG. 1: Experimental setup. Electrons and ions are created in the supersonic gas-jet target. The thin copper rings create a homogeneous electric field and the large Helmholtz coils an additional magnetic field. These fields guide the charged particles onto fast time and position sensitive channel plate detectors (Roentdek, www.roentdek.com). The time-of-flight (TOF) and the position of impact of each electron-ion pair is recorded in list mode. From this the three dimensional momentum vector of each particle can be calculated.

gas-jet as target. More recently, atoms in magneto-optical traps have been used to further increase the resolution [13–16].

A typical setup as it was used for the experiments discussed here is shown in figure 1. The laser pulse is focused by a lens of $5cm$ focal length or a parabolic mirror into a supersonic gas-jet providing target atoms with very small initial momentum spread of below $0.1au$ (atomic units are used throughout this paper) in the direction of the laser polarization (along z-axis in figure 1). For experiments in ion-atom collisions or with synchrotron radiation the ionization probability is very small: That's why one aims at a target density in the range of up to $10^{-4}mbar$ local pressure in the gas-jet. Accordingly, a background pressure in the chamber in the range of $10^{-8}mbar$ is sufficient. In contrast for multiple ionization by femtosecond laser pulses the single ionization probability easily reaches unity. Thus, within the reaction volume defined by the laser focus of typically $(10\mu m)^2 \cdot 100\mu m$ all atoms are ionized. Since for coincidence experiments it is essential that much less than one atom is ionized per laser shot a background pressure of less than $10^{-10}mbar$ is required. The gas-jet

has to be adjusted accordingly to reach single collision conditions at the desired laser peak power. With standard supersonic gas-jets this can only be achieved by tightly skimming the atomic beam, since a lower driving pressure for the expansion would result in an increase of the internal temperature of the jet along its direction of propagation. Single ionization (see section III) allows for an efficient monitoring of the resolution as well as online controlling of single collision conditions.

The ions created in the laser focus are guided by a weak electric field towards a position sensitive channel plate detector. From the position of impact and the time-of-flight (TOF) of the ion all three components of the momentum vector and the charge state are obtained. A typical ion TOF spectrum from the experiment reported in [17] is shown in figure 2.

The electric field also guides the electrons towards a second position sensitive channel plate detector. To collect electrons with large energies transverse to the electric field a homogeneous magnetic field is superimposed parallel to the electric field. This guides the electrons on cyclotron trajectories towards the detector. Depending on their time-of-flight the electrons perform several full turns on their way to the detector. Figure 3 shows the electron TOF versus the radial distance of the position from a central trajectory with zero transverse momentum of the electron. When the TOF is an integer multiple of the cyclotron frequency the electrons hit the detector at his position, independently of their momentum transverse to the field. These TOFs represent points in phase space where the spectrometer has no resolution in the transverse direction. For all other TOFs the initial momentum can be uniquely calculated from the measured positions of impact and the TOF. Using a magnetic field of 10 Gauss 4π solid angle collection is achieved for electrons up to about $30eV$. The typical detection probability of an electron is in the range of 30%-40%. Thus, even for double ionization in most cases only one electron is detected. The positions of impact and the times-of-flight are stored for each event in list mode. Thus the whole experiment can be replayed in the offline analysis. A detailed description of the integrated multi-electron-ion momentum spectrometer can be found in [18].

III. SINGLE IONIZATION AND THE TWO-STEP MODEL

The momentum distribution of singly charged helium ions produced by absorption of one $85eV$ photon (synchrotron radiation) and by multiphoton absorption at $800nm$ and

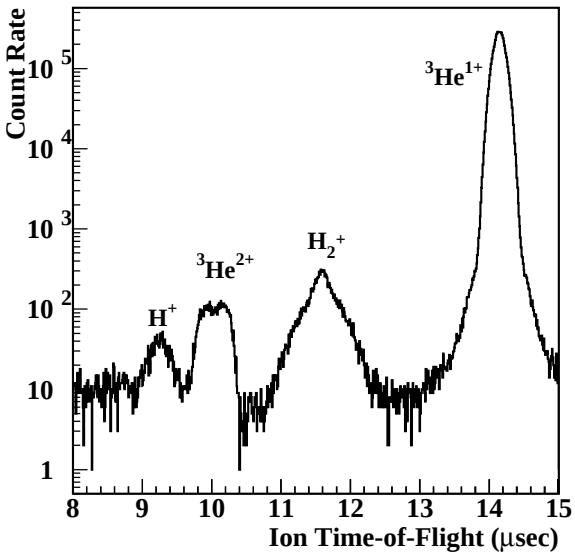

FIG. 2: Time-of-flight distribution of ions produced by a $6.6 \cdot 10^{14} W/cm^2$ laser pulse. The gas target was ^3He; the residual gas pressure in the chamber was about $2 \cdot 10^{-10} mbar$. The double peak structure in the $^3He^{2+}$ peak can be seen. The total count rate was about 0.1 ion per laser shot.

$1.5 \cdot 10^{15} W/cm^2$ is shown in figure 4. In both cases the momentum of the photon is negligible compared to the electron momentum. Therefore, electron and He^{1+} ion are essentially emitted back-to-back compensating each others momentum (The exact kinematics including the photon momentum can be found in [9] section 2.3.1..). Hence, for single ionization the spectroscopy of the ion momentum is equivalent to electron spectroscopy. This can be directly confirmed by looking at the coincidence between the ions and electrons in figure 5. All true coincidence events are located on the diagonal with equal momenta p_z in the TOF direction. The width of this diagonal gives the combined resolution of the electron and ion momentum measurement for the p_z component (in this case $0.25 au$ full width at half maximum). All events off the diagonal result from false coincidences in which the electron and ion were created in the same pulse but did not emerge from the same atom. This allows a continuous monitoring of the fraction of false coincidences during the experiment. Knowing this number the false coincidences can also be subtracted for double ionization

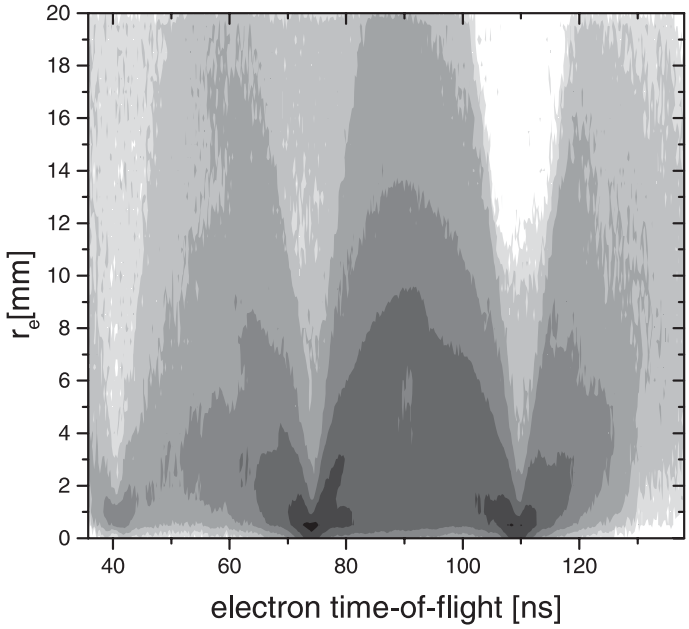

FIG. 3: Horizontal axis: Electron time-of-flight. Vertical axis: radial distance from a central trajectory with zero transverse momentum on electron detector, see text.

events.

For single photon absorption the electron energy is uniquely determined by the photon energy E_γ and the binding energy plus a possible internal excitation energy of the ion. The resulting narrow lines in the photoelectron energy spectrum correspond to spheres in momentum space. The left panel of figure 4 shows a slice through this momentum sphere. The outer ring corresponds to He^{1+} ions in the ground state, the inner rings to the excited states. The photons are linearly polarized with the polarization direction horizontal in the figure. The angular distribution of the outer ring shows an almost pure dipole distribution according to the absorption of one single photon. Contrary, in the laser field any number of photons can be absorbed, leading to an almost continuous energy distribution of the electrons (right panel in figure 4). Structure of individual ATI (above threshold ionization) peaks spaced by the photon energy ($1.5eV$) is not seen here. This is in agreement with electron spectra , where at comparable laser intensities ATI structure is not observed, either. The electrons and ions are emitted in narrow jets along the polarization axis. Such high angular momentum states, needed to produce this kind of distribution, are accessible due to the large number of photons absorbed.

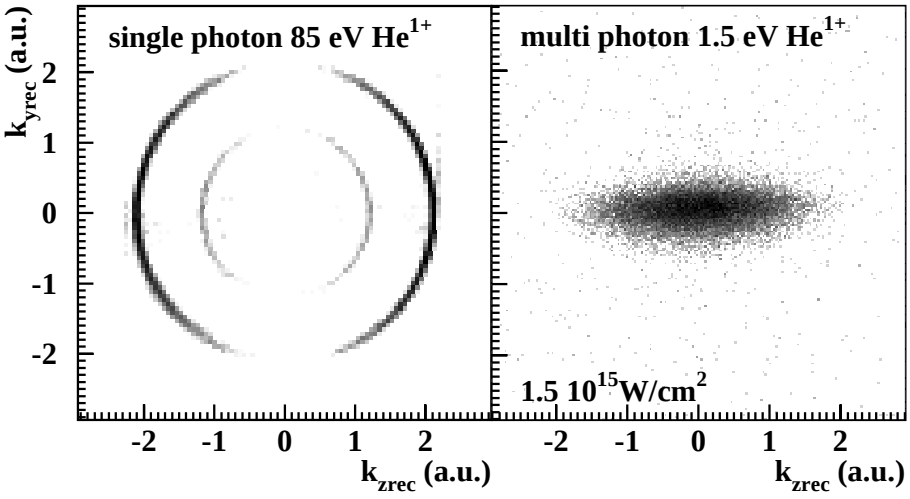

FIG. 4: Momentum distribution of He^{1+} ions. Left: For $85eV$ single photon absorption. Right: $1.5eV$ $(800nm)$, 220 fsec, $1.5 \cdot 10^{15} W/cm^2$. The polarization vector of the light is horizontal. The photon momentum is perpendicular to the (k_y, k_z) plane. In the left figure the momentum component in the third dimension out of the plane of the figure is restricted to $\pm 0.4au$. The right panel is integrated over the momenta in the direction out of the plane of the figure.

How do the ions and electrons get their momenta? For the case of single photon absorption the light field is so weak that there is no acceleration. Also, the photon carries no significant momentum into the reaction. The photon cuts the tie between nucleus and electron by providing the energy. The momenta observed in the final state thus have to be present already in the initial state Compton profile of the atom. Single photon absorption is therefore linked to a particular fraction of the initial state wave function, which in momentum representation coincides with the final state momentum. The scaling of the photo ionization cross section at high energies follows, besides a phase factor, the initial state momentum space Compton profile, i.e. the probability to find an electron-ion pair with the appropriate momentum in the initial state.

In the strong field case the situation changes completely. The field is strong enough to accelerate the ions and electrons substantially after the electron is set free. The momentum balance, however, is still the same as in the single photon limit: The laser field accelerates electron and ion to the opposite directions resulting again in their back-to-back emission

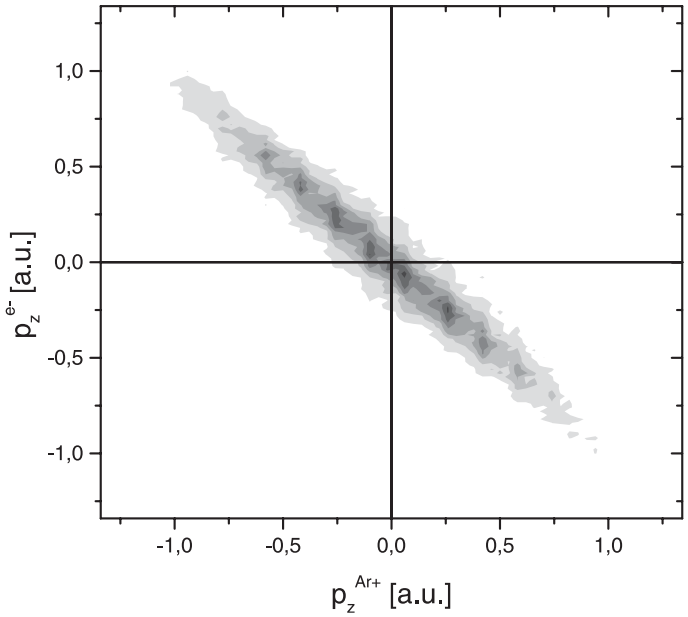

FIG. 5: Single ionization of argon by $3.8 \cdot 10^{14} W/cm^2$. The horizontal axis shows the momentum component of the recoil ion parallel to the polarization. The vertical axis represents the momentum of the coincident electron in the same direction. By momentum conservation all true coincidences are located on the diagonal. Along the diagonal ATI peaks can be seen. The z-axis is plotted in linear scale.

(see figure 5). This changes only if the laser pulse is long enough, such that the electron can escape from the focus during the pulse. Then, a case which we do not consider here, the momenta are balanced by a huge amount of elastically scattered photons. In the regime of wavelength and binding energies under consideration here, a simple two-step picture has been proven useful. In the first step the electron is set free by tunneling through the potential barrier created by the superposition of the Coulomb potential of the atom and the electric field of the laser. This process promotes electrons and ions with zero momentum to the continuum. Then they are accelerated in the laser field and perform a quiver motion. In this model the net momentum in the polarization direction, which is observed after the pulse with an envelope of the electric field strength E(t) being long to the laser frequency, is purely a function of the phase of the field at the instant of tunneling (tunneling time t_0):

$$p_z^{He^{1+}}(t_\infty) = \int_{t_0}^{t_\infty} E(t) \sin \omega t \, dt \qquad . \tag{1}$$

Tunneling at the field maximum thus leads to electrons and ions with zero momentum.

The maximum momentum corresponding to the zero crossing of the laser field is $\sqrt{4U_p}$, where $U_p = I/4\omega^2$ is the ponderomotive potential at an intensity I and photon frequency ω ($U_p = 39.4\,eV$ at $6.6{\cdot}10^{14} W/cm^2$). Within this simple model the ion and electron momentum detection provides a measurement of the phase of the field at the instant of tunneling. We will generalize this idea below for the case of double ionization.

Single ionization is shown here mainly for illustration. Much more detailed experiments have been reported using conventional TOF spectrometers (see [4] and references therein) and photoelectron imaging [19, 20].

IV. MECHANISMS OF DOUBLE IONIZATION

What are the "mechanisms" leading to double ionization? This seemingly clear-cut question does not necessarily have a quantum mechanical answer. The word "mechanism" mostly refers to an intuitive mechanistical picture. It is not always clear how this intuition can be translated into theory and even if one finds such a translation the contributions from different mechanisms have to be added coherently to obtain the measurable final state of the reaction [21, 22]. Thus, only in some cases mechanisms are experimentally accessible. This is only the case if different mechanisms occur at different strengths of the perturbation (such as laser power or projectile charge) or if they predominantly populate different regions of the final state phase space. In these cases situations can be found where one mechanism dominates such that interference becomes negligible. With these words of caution in mind, we list the most discussed mechanisms leading to double ionization:

1. **TS2 or Sequential Ionization:** Here the two electron are emitted sequentially by two independent interactions of the laser field with the atom. From a photon perspective one could say that each of the electrons absorbs photons independently. From the field perspective one would say that each electron tunnels independently at different times during the laser pulse. This is equivalent to the TS2 (two-step-two) mechanism in ion-atom and electron-atom collisions. In this approximation the probability of the double ejection can be estimated in an independent particle model. Most simply one calculates double ionization as two independent steps of single ionization. A little more refined approach uses an independent event model, which takes into account the

different binding energies for the ejection of the first and the second electron (see e.g. [23] for ion impact, [24] for laser impact).

2. **Shake-Off:** If one electron is removed rapidly (sudden approximation) from an atom or a molecule, the wave function of the remaining electron has to relax to the new eigenstates of the altered potential. Parts of these states are in the continuum, so that a second electron can be "shaken off" in this relaxation process. This is known for example from beta decay, where the nuclear charge is changed. Shake-off is also known to be one of the mechanisms for double ionization by absorption or Compton scattering of a single photon (see the discussion in [25] and references therein). However, only for very high photon energies (in the keV range) it is the dominating mechanism. For helium it leads to a ratio of double to single ionization of 1.66% [26, 27] for photoabsorption (emission of the first electron from close to the nucleus) and 0.86% for Compton scattering (averaged over the initial state Compton profile) [28].

3. **Two-Step-One (TS1):** For single photon absorption at lower photon energies (threshold to several $100eV$ [22]) TS1 is known to dominate by far over the shake-off contribution. A simplified picture of TS1 is that one electron absorbs the photon and knocks out the second one via an electron-electron collision on its way through the atom [29]. A close connection between the electron impact ionization cross section and the ratio of double to single ionization by single photon absorption as function of the energy is seen experimentally [29] and theoretically [22], supporting this simple picture. For the TS1 mechanism the electron correlation is on a very short time scale (a few attoseconds) and confined to a small region of space (the size of the electron cloud).

4. **Rescattering:** Rescattering is a version of the TS1 mechanism which is induced only by the laser field. The mechanism was proposed originally by Kuchiev [30] under the name "antenna model". He suggested that one of the electrons is driven in the laser field acting as an antenna absorbing the energy which it then shares with the other electron via correlation. Corkum [31] and Schafer [32] extended this basic idea and interpreted the process in the two step model: First one electron is set free by tunneling. Then it is accelerated by the laser field and is driven back to its parent ion with about 50% probability. Upon recollision with the ion the electron can recombine

and emit higher harmonic radiation. Besides that it could be elastically scattered and further accelerated or it could be inelastically scattered with simultaneous excitation or ionization of the ion. In contrast to TS1 in this case there is a femtosecond time delay between the first and the second step. Also the wave function of the rescattered electron explores a larger region of space than in the case of TS1 [33–35].

A strong experimental evidence favoring the rescattering process to be dominantly responsible for double ionization by strong laser fields was later provided by the observation that double ejection is strongly suppressed in ionization with circularly polarized light [36, 37] (see also figure 19 in [3]). The rescattering mechanism is inhibited by the circular polarization since the rotating electric field does not drive the electrons back to their origin. The other mechanisms, in contrast, are expected to be polarization independent.

To gain further insight in the double ionization process clearly differential measurements beyond the ion yield are necessary. Two types of such experiments have been reported recently: Electron time-of-flight measurements in coincidence with the ion charge state [38, 39] and those using COLTRIMS, where at first only the ion momenta [40–42] and later the ion momenta in coincidence with one electron [17, 43–45] have been measured.

V. RECOIL ION MOMENTA

A. From nonsequential to sequential double ionization

Recoil ion momentum distributions have been measured for helium (He^{1+},He^{2+}) [40], neon (Ne^{1+},Ne^{2+},Ne^{3+}) [41] and argon (Ar^{1+},Ar^{2+}) [45, 46]. Figure 6 summarizes some of the results for neon. The momentum distribution of the singly charged ion is strongly peaked at the origin like in the case of helium (figure 4), reflecting the fact that tunnel ionization is most likely at the maximum of the field (see equation 1). The structure of the momentum distribution of the doubly charged ions changes strongly with the peak intensity. In the region where the rates suggest the dominance of nonsequential ionization the ion momenta show a distinct double peak structure (figure 6(2)). At higher intensities, where rates can be described by assuming sequential ionization, the momenta of the Ne^{2+} ions are peaked at the origin like for single ionization. The studies for helium show a similar double peak structure at $6.6 \cdot 10^{14} W/cm^2$ (see figure 9).

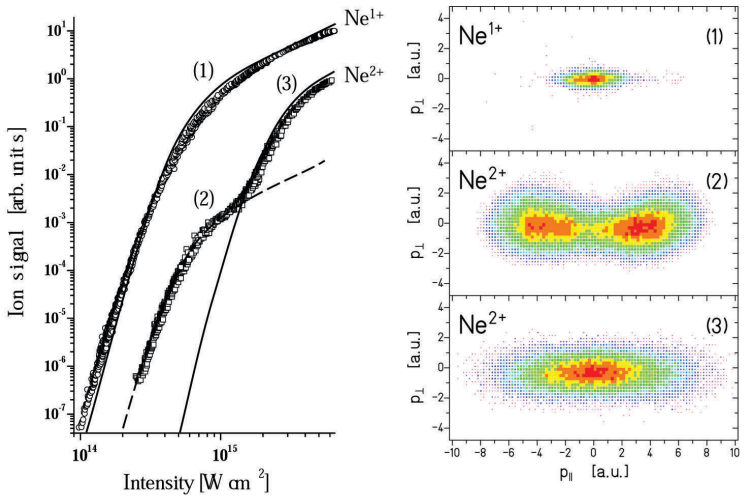

FIG. 6: Neon double ionization by $800nm$, $25fs$ laser pulses. Left panel: Rate of single and double ionization as a function of the laser power (from [47]). The full line shows the rate calculated in an independent event model. Right panel: Recoil ion momentum distributions at intensities marked in the left panel. A projection of the double peaked distribution (2) is shown in figure 10. Horizontal axis: Momentum component parallel to the electric field. Vertical axis: One momentum component perpendicular to the field (data partially from [48])

.

The evolution of the ion momentum distributions with laser peak power has been studied in detail for argon [46], too, confirming the fact that at the transition to the nonsequential regime an increase in laser power results in colder ions. The argon data, however, show no distinct double peak structure (see figure 7), where the sequential ionization already sets in at about $6.6 \cdot 10^{14} W/cm^2$. The reason might be, that the sequential contribution fills "the valley" in the momentum distribution at the origin before a double peak structure has developed. In [45] it has been argued based on classical kinematics that excitation of a second electron during recollision followed by tunneling ionization of the excited electron might be responsible for "filling the valley". Due to the open 3d shell in Ar, excitation cross sections are much larger than in Ne. At the highest intensity the single peak distribution can be at least qualitatively understood in an independent two step picture (see figure 7). The dash-dotted lines in figure 7 show the measured momentum distributions of Ar^{1+} ions, the dashed line this distribution convoluted with itself. Such convolution models two

sequential and totally uncorrelated steps of single ionization spaced in time by a random number of optical cycles. Figure 7 shows that for argon at $12 \cdot 10^{14} W/cm^2$ (which, judging from the rates, is in the sequential regime), this very simple approach describes the ion momentum distributions in double ionization rather well. One obvious oversimplification of this convolution procedure is that it implicitly assumes that the momentum distributions do not change with binding energy. A more refined independent event approach would use different binding energies for both steps. As an alternative simple model, the momentum distribution for for removal of the first electron and the second electron have been calculated in the ADK (Ammosov, Delone, Krainov) model (see e.g. [49] equation 10) using the correct binding energies for both steps. The result of convoluting these two calculated distributions is shown by the full lines in figure 7. Clearly such modeling fails in the regime where sequential ionization dominates (figure 7a).

B. The origin of the double peak structure

The recoil ion is an important messenger carrying detailed information on the time evolution of the ionization process. It allows not only to distinguish between sequential and nonsequential ionization but also to rule out some of the nonsequential mechanisms as we will show now.

Analogous to the situation for single ionization discussed above one can estimate the net momentum accumulated by the doubly charged ion from the laser pulse as

$$p_z^{He^{2+}}(t_\infty) = \int_{t_1}^{t_{12}} E(t) \sin \omega t dt + 2 \int_{t_{12}}^{t_\infty} E(t) \sin \omega t dt. \qquad (2)$$

The first electron is removed at time t_1 and the ion switches its charge from 1+ to 2+ at time t_{12}. It is assumed that there is no momentum transfer to the ion from the first emitted electron during double ionization. Thus, as in the case of single ionization the phase of the field at the instant of the emission of the first and of the second electron is encoded in the ion momentum.

Shake-off and TS2 will both lead to a momentum distribution peaked at zero, similar to single ionization. In both cases the emission of the second electron follows the first with a time delay, which is orders of magnitude shorter than the laser period. Hence $t_{12} = t_1$ in equation 2 and since the first electron is emitted most likely at the field maximum $p_z^{He^{2+}}$

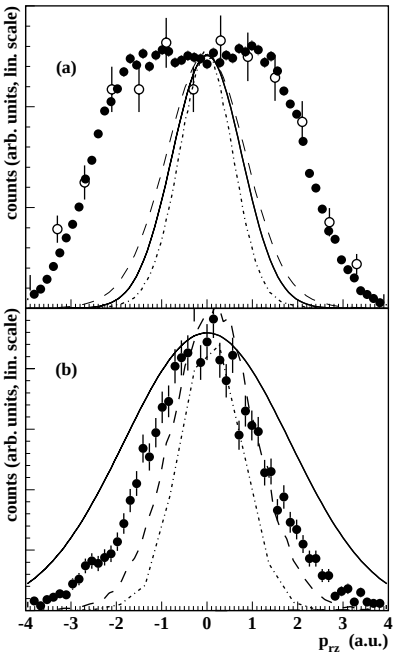

FIG. 7: Momentum distribution of Ar^{2+} ions created in the focus of a $220fs$, $800nm$ laser pulse at peak intensities of $3.75 \cdot 10^{14} W/cm^2$ (a) and $12 \cdot 10^{14} W/cm^2$ (b) in the direction of the polarization. The distributions are integrated over the directions perpendicular to the polarization: full circles: distribution of Ar^{2+} ions; dotted line: distribution of Ar^{1+} ions; dashed line: results of the independent electron model of convoluting the Ar^{1+} distribution with itself; full line: results of the independent electron ADK model (see text); open circles in (a): distribution of He^{2+} ions at $3.8 \cdot 10^{14} W/cm^2$ (figure from [46], helium data from [40]).

would also peak at zero for shake-off and TS1. Consequently, the observed double peak structure for He and Ne directly rules out these mechanisms.

For the rescattering there is a significant time delay between the emission of the first electron and the return to its parent ion. Estimating t_{12} for a rescattering trajectory which has sufficient energy to ionize leads to ion momenta close to the measured peak positions [40, 41, 50]. The high momenta of the doubly and triply charged ions are a direct proof of the time delay introduced by the rescattering trajectory. It is this time delay with respect to the field maximum, which is responsible for multiple ionization and allows an effective net momentum transfer to the ion by accelerating the parent ion. Within the classical rescattering model the final momentum of the doubly charged ion will be the momentum

received from the field (as given by equation 2) plus the momentum transfer from the recolliding electron to the ion.

Soon after the measurement of the first ion momentum distributions Becker and Faisal succeeded in the first theoretical prediction of this quantity. They calculated double ionization of helium using (time independent) S-matrix theory. They evaluated the Feynman diagram shown in figure 8. Time progresses from bottom to top. Starting with 2 electrons in the helium ground state at time t_i, the laser field couples once at t_1 to electron 1 (V_{ATI}). Electron 1 is then propagated in a Volkov state (k) in the presence of the laser field, while electron 2 is in the unperturbed He^{1+} ground state (j). Physically the Volkov electron does not have a fixed energy but can pick up energy from the field. This describes e.g. an acceleration of the electron in the field and its return to the ion. At time t_2 one interaction of the two electrons via the full Coulomb interaction is included. This allows for an energy transfer from the Volkov electron to the bound electron. Finally, both electrons are propagated independently in Volkov states, describing their quiver motion in the field. By evaluating this diagram Becker and Faisal obtained excellent agreement with the observed ion yields (see [52, 53] for helium and [54] for an approximated rate calculation on other rare gases). The ion momentum distribution calculated as the sum momentum of the two electrons predicted by this diagram is shown in figure 9b. The calculation correctly predicts the double peak structure and the position of the maxima. The minimum at momentum zero is more pronounced in the calculation than in the data. The major approximations, which might be responsible for this are: Only one step of electron-electron energy transfer is taken into account (see [55] for a discussion of the importance of multiple steps); no intermediate excited states are considered and the laser field is neglected for all bound states as in turn the Coulomb field is neglected in the continuum states. To unveil the physical mechanism producing the double hump structure Becker and Faisal have evaluated the diagram also by replacing the final Volkov states by plane waves. Physically this corresponds to switching off the laser field after both electrons are in the continuum. In the calculation this lead to a collapse of the double peak structure to a single peak similar to single ionization. This confirms our interpretation given above, that it is the acceleration of the ion in the field after the rescattering (starting at t_{12} in equation 2), which leads to the high momenta. The S-matrix theory also yielded good agreement with the observed narrow momentum distribution in the direction perpendicular to the laser field.

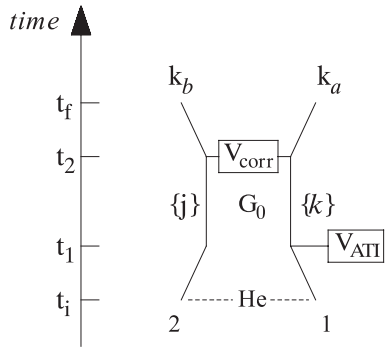

FIG. 8: Feynman diagram describing the rescattering and TS1 mechanism (from [51]). See text.

Later, different approximations in the evaluation of the diagram (figure 8) have been introduced. First, Kopold and coworkers [56] replaced the electron-electron interaction by a contact potential and additionally used a zero range potential for the initial state. This simplified the computation considerably and still they obtained the observed double peak structure not only for helium but also for neon (figure 10b) and other rare gases. They found that the inclusion of intermediate excited states of the singly charged ion yields a filling of the minimum at zero momentum.

Goreslavskii and Popruzhenko [57, 58] used the saddle point approximation for the intermediate step. This additional approximation did not change the calculated ion momenta strongly (see figure 9c) but simplified the computation, allowing to investigate also the correlated electron emission discussed in the next section.

A conceptionally very different approach was used by Sacha and Eckhardt [60]. They argued that the rescattering will produce a highly excited intermediate complex, which will then decay in the presence of the field. This decay process will not have any memory of how it was created. They assumed a certain excitation energy as free parameter in the calculations and then propagated both electrons in the classical laser field semiclassically in reduced dimensions. Therefore they analyzed this decay by a Wannier type analysis.

Wannier theory is known to reproduce the electron angular dependence as well as the recoil ion momenta for the case of single photon double ionization [25, 61–63]. In this case the Wannier configuration would be the emission of both electrons back-to-back, leaving the recoil ion at rest on the saddle of the electron-electron potential. For single photon absorption from an S state this configuration is forbidden by selection rules, it would allow,

however, the absorption of an even number of photons.

In the multiphoton case the external field has to be included in addition to the Coulomb potential among the particles. This leads to a saddle in the potential, which is not at rest at the center between the electrons but at momenta which correspond to the observed peaks. Sacha and Eckhardt analyzed classical trajectories in the saddle potential created by the field and the Coulomb potentials. At a given laser field the decay of the excited complex in the field is characterized only by two parameters: The time when the complex is created and the total energy. Interestingly the recoil ion momentum obtained this way exhibits a double peak structure, which does not depend strongly on the creation time but on the energy. They find parallel and perpendicular momentum distributions, which are for helium (figure 9f) and neon (figure 10c) in reasonable agreement with the experiment. This argument of a time independent intermediate complex seems to contradict the claim that the high recoil momenta and the double peak are a result of the time delay due to the rescattering. One has to keep in mind, however, that within the rescattering model the recollision energy and hence the total energy of the complex analyzed by Sacha and Eckhardt is uniquely determined by the recollision time. In a recent work they extended this model to examine the decay of highly excited three electron atoms [64].

The S-matrix approaches discussed above are based on the time independent Schrödinger equation. One of the advantages of such approaches is, that it allows a precise definition of a mechanism (see e.g. [10]). Each particular diagram represents one mechanism. The price that has to be paid is the loss of information on the time evolution of the system. The diagram contains the time order of interactions, but not the real time between them. Starting from the time dependent Schrödinger equation in contrast gives the full information on the time evolution of the many body wave function in momentum or coordinates space. In these coordinate space density distributions it is, however, often difficult to clearly define what one means with a mechanism. Lein and coworkers found a very elegant way to solve this problem [34, 35]. Instead of plotting the density in coordinates space they calculated the Wigner transform of the wave function, depending on momentum and position. Integrated over the momentum coordinate it is the density in coordinate space and integrated over the position it is the the distribution in momentum space. The Wigner transform can be read as a density in phase space. Lein and coworkers plotted for example the phase space evolution of the recoil ion in the polarization direction. This presentation of a quantum mechanical

wave function is very close to the presentation of the classical phase space trajectories. The rescattering mechanism can be seen very clearly in this presentation.

Computation of the time dependent Schrödinger equation for three particles in three dimensions is extremely challenging. Even though great progress has been made in this field (see e.g. [65–70]), there are no predictions of recoil ion momenta or other differential information based on the solution of the time dependent Schrödinger equation in three dimensions for the "long" wavelength regime of presently available high-intensity lasers.

To allow for a practical calculation of the time evolution of the three body system two rather different approximations have been made: a) Reducing the dimensions from three for each particle to only one along the laser polarization and b) keeping the full dimensionality but using classical mechanics instead of the Schrödinger equation [71].

Lein et al [34] reported the first results on recoil ion momenta based on an integration of the one-dimensional Schrödinger equation (see figure 9d). The momentum distribution of the He^{2+} ions at $6.6 \cdot 10^{14} W/cm^2$ in figure 9d) peaks at zero momentum in contrast to all other results. It will become clear in section VII that there is evidence in Lein et al's calculation for a correlated emission of both electrons into the same hemisphere. A well known problem of one-dimensional calculations is that the effect of electron repulsion is overemphasized. This might be partially responsible for "filling the valley" in these calculations. For further discussion see section VII.

Chen et al [59] have performed a Classical Trajectory Monte Carlo calculation (CTMC) in which they solved the classical Hamilton equations of motion for all three particles in the field. Instead of a full classical simulation of the process (see e.g. [72] for CTMC calculation for single ionization and [71] for refined classical calculation of double ionization rates) they have initialized one electron by tunneling and then propagated all particles classically. This also yields the observed double peak structure. Such CTMC calculations have proven to be extremely successful in predicting the highly differential cross sections from ion impact single and multiple ionization (see [73–80] for some examples). One of the virtues of this approach is that the output comprises the momenta for each of the particles for each individual ionizing event, exactly like in a COLTRIMS experiment. In addition, however, each particle can be followed in time shedding light on the mechanism. Such detailed studies would be highly desirable for the strong field case, too.

All theoretical analysis of the observed double peak structure in the recoil ion distribution

confirms the first conclusion from both experimental teams reporting these structures: a) It is an indication of the nonsequential process and b) it is consistent with the rescattering mechanism, which is included in one or the other way in the various theoretical models.

In the direction perpendicular to the polarization the observed and all calculated distributions are very narrow and peak at zero. Since there is no acceleration by the laser field in this direction the transverse momentum of the ion is purely either from the ground state or from the momentum transfer in the recollision process. All theories, which are not confined to one dimension, roughly agree with the experimental width of the distribution. This direction should be most sensitive to the details of the recollision process since that is where the parallel momentum acquired from the field is scattered to the transverse direction. Hence, a closer inspection of the transverse momentum transfer is of great interest for future experimental and theoretical studies.

VI. ELECTRON ENERGIES

Electron energy distributions for double ionization have been reported for helium [39], argon [81], neon [82] and xenon [38]. All these experiments commonly find in the sequential regime that the electron energies from double ionization are much higher than those generated in single ionization. This is in full agreement with the recoil ion momenta discussed above, since the mechanism being predominantly responsible for producing high energy electrons is exactly the same: It is fact that due to the rescattering the electrons from double ionization are not promoted to the continuum at the field maximum but at a later time. Depending on the actual time delay an energy of up to $2U_p$ (see equation 1) can be acquired. The work for helium (figure 11) and neon shows that the electron spectra extend well above this value. Energies beyond $2U_p$ are only obtainable if the recolliding electron is backscattered during the (e,2e) collision. In this case the momentum, which they have after the recollision adds to the momentum acquired in the field. A large amount of elastically backward scattered electrons has been observed for single ionization where a plateau in the energy distribution is found extending to energies of up to $10U_p$.

VII. CORRELATED ELECTRON MOMENTA

More information can be obtained from the momentum correlation between the two electrons. In an experiment one possible choice would be to observe the momenta of both electrons in coincidence. In this case the recoil ion momentum could be calculated employing momentum conservation. From an experimental point of view however, it is easier to detect the ion and one of the electrons, in which case the momentum of the second electron can be inferred from momentum conservation. It is experimentally simpler, since the additional knowledge of the ion charge state, allows for an effective suppression of random coincidences. Moreover, electron and ion are detected on opposite detectors circumventing possible problems of multihit detection. Many successful studies for single photon double ionization have been performed this way [25, 63, 83, 84]. Up to present, however, no fully differential experiment has been reported for multiphoton double ionization. Weber et al [17] and Feuerstein et al [45] reported measurements observing only the momentum component parallel to the field of electron and ion integrating over all other momentum components. Weckenbrock et al [43] and Moshammer [48] have detected the transverse momentum of one of the electrons in addition to the parallel momenta. In these experiments, however, the transverse momentum of the ion could not be measured with sufficient resolution, mainly due to the internal temperature of the gas-jet for argon and neon targets. Experiments on helium have not jet been reported but are in preparation in several laboratories.

A. Experimental findings

The correlation between the momentum components parallel to the polarization is shown in figure 12. The electron momenta are integrated over all momentum components perpendicular to the field direction. Events in the first and third quadrant are those where both electrons are emitted to the same hemisphere, the second and fourth quadrant correspond to emission to opposite half spheres. The upper panel shows the electron momenta at an intensity of $3.6 \cdot 10^{14} W/cm^2$, which is in the regime where nonsequential ionization is expected. The distribution shows a strong correlation between the two electrons, they are most likely emitted to the same hemisphere with a similar momentum of about $1au$. At higher intensity, where double ionization proceeds sequentially this correlation is lost (lower

panel in figure 12).

To interpret the correlation pattern it is helpful to consider the relationship between the electron and the recoil ion momenta. We define the Jacobi momentum coordinates k_z^+ and k_z^-:

$$k_z^+ = k_{ez1} + k_{ez2} \tag{3}$$

$$k_z^- = k_{ez1} - k_{ez2} \tag{4}$$

with $k_{zion} = -k_z^+$. These coordinates are along the diagonals of figure 12. Hence the recoil ion momentum distribution is simply a projection of figure 12 onto the diagonal k_z^+. The coordinates k_z^+ and k_z^- are helpful to illustrate the relative importance of the two counteracting effects of electron-electron repulsion and acceleration of particles by the optical field. Both influence the final state momenta in different ways. Electron repulsion (and two-body electron-electron scattering) does not change k_z^+ but contributes to the momentum k_z^-. On the other hand, once both electrons are set free, the momentum transfer received from the field is identical for both. Therefore, this part of the acceleration does not change k_z^- but adds to k_z^+. The observed wide k_z^+ and narrow k_z^- distributions thus indicate that the joint acceleration of the electrons in the laser field clearly dominates over the influence of electron repulsion.

For argon double ionization Weckenbrock et al [43] and Moshammer et al [85] measured in addition to the momentum parallel to the field also the transverse momentum of the detected electron. Both find that the correlation pattern strongly depends on this transverse momentum (see figure 13). If one electron is emitted with any transverse momentum larger than $0.1au$ (i.e. with some angle to the polarization axis) one mostly finds both electrons with a similar momentum component in the field direction. It is this configuration which dominates the integrated spectrum in figure 12. If, however, one electron is emitted parallel to the polarization with a very small transverse momentum window of $p_\perp < 0.1au$ one finds that the parallel momentum distribution does no longer peak on the diagonal. In this case most likely one electron is fast and the other slow. This might be due to the fact that the $1/r_{12}$ potential forces the electrons into different regions in the three dimensional phase space. Consequently, for electrons to have equal parallel momentum some angle between them is required. Accordingly, the peak at $p_{ez1} = p_{ez2} = 1au$ is found to be most pronounced if at least one of the electrons has considerable transverse momentum. In tendency, this feature

can be explained by (e,2e) kinematics as discussed in [85]: Unequal momentum sharing is known to be most likely in field free (e,2e) reactions. The rescattered electron is only little deflected losing only a little of its longitudinal momentum during recollision. At the same time, the ionized electron is low-energetic resulting in very different start momenta of both electrons at recollision time t_{12}. At intensities not too close to the threshold this scenario leads to asymmetric longitudinal energy sharing as calculated in [57, 86].

B. Comparison to single photon and charged particle impact double ionization

One might expect that the pure effect of electron repulsion could be studied in double ionization by single photon absorption with synchrotron radiation. In this case there is no external field in the final state that could accelerate the electrons. Many studies have shown however, that the measured momentum distribution is not only governed by the Coulomb forces in the final state, but also by selections rules resulting from the absorption of one unit of angular momentum and the accompanying change in parity. For helium for example the two electron continuum wave function has to have $^1P^o$ character. Since these symmetry restrictions on the final state are severe it is misleading to compare distributions of k_{ez1} versus k_{ez2} as in figure 12 directly to those from single photon absorption (this distribution can be found in [87]). The effect of electron repulsion can be more clearly displayed in a slightly different geometry as shown in figure 14. Here one electron is emitted along the positive x direction and the momentum distribution of the second electron is shown. The data are integrated over all directions of this internal plane of the three body system relative to the laboratory. Clearly electron repulsion dominates the formation of this final state distribution, there is almost no intensity for emission to the same half sphere. There is also a node for emission of both electrons back-to-back. This is a result of the odd symmetry of the final state. In the multiphoton case this node is expected for those events where an odd number of photons is absorbed from the field (see e.g. [88]).

Another instructive comparison is the process of double ionization by charged particle impact. Experiments have been reported for electron impact [90–92] and fast highly charged ion impact [80, 93]. The latter is of particular interest from the strong field perspective since the potential "shock" induced at a target atom by a fast highly charged projectile is in many aspects comparable to a half cycle laser pulse. The time scale however is much shorter

than the one accessible with lasers today. For their experiment colliding 1 GeV/u U^{92+} projectiles on helium for example Moshammer and coworkers [94] estimated a power density of $> 10^{19} W/cm^2$ and a time of sub attoseconds. Under such conditions ion-atom collisions can be successfully described by the Weizsäcker-Williams formalism [94–97], which replaces the ion by a flash of virtual photons (for a detailed discussion on the validity and limitations of this method see [98]). Since such an extremely short "photon field" also has contributions from very high frequencies, i.e. virtual photon energies, the ionization is dominated by the absorption of one photon per electron. This is contrary to the femtosecond laser case discussed here. Multiple ionization in fast ion-atom collisions is either dominated by the TS2 or the TS1 process (with only a small amount of shake-off) depending on the strength of the perturbation, i.e. the intensity of the virtual photon field. The ratio of the projectile charge over the projectile velocity is usually taken as a measure of the perturbation. Figure 15 shows the electron momentum correlation of double ionization of helium by $100 MeV/u\ C^{6+}$ impact parallel to the direction of the projectile. The dominant double ionization mechanism at these small perturbations is TS1 [99], or, in a virtual photon picture, one photon is absorbed during a collision by either one of the electrons and the second is taken to the continuum due to electron-electron correlation. Under these conditions the electron repulsion in the final state drives the electrons to opposite half spheres, whereas the projectile itself passes so fast that during this short time essentially no momentum is transferred to the system. Similar studies have been performed with slower and more highly charged projectiles [80]. In this case the dominant double ionization mechanism is TS2. The experiments show a joint forward emission of both electrons. This effect has been interpreted in a two-step picture: First the initial state momentum distribution is lifted to the continuum by absorption of two virtual photons and in a second step the strong potential of the projectile accelerates both electrons into the forward direction (see also [97] for a theoretical interpretation of the double ionization process; see [100] for another experiment showing directed multiple electron emission and see [79] for an analysis of the acceleration of an electron in the field of the projectile).

C. Interpretation within the rescattering model

The data shown in figure 12 can be qualitatively understood by estimating the momentum transfer in the rescattering model. From this one obtains kinematical boundaries of the momenta for different scenarios. For simplicity we restrict ourselves to a single return of the electron.

If the electron recollides with an energy above the ionization threshold clearly double ionization is possible. The electron will loose the energy (and hence the momentum) necessary to overcome the binding of the second electron. The remaining excess energy can be freely distributed among the two electrons in the continuum. From electron impact ionization studies it is known that the electron energy distribution is asymmetric, i.e. one fast, one slow electron is most likely, for excess energies above 10 to $20eV$. The momentum vector of the electrons can point in all directions, however, forward scattering of one electron is most likely (see [101] for a review of electron impact ionization). After recollision the electrons are further accelerated in the field yielding a net momentum transfer at the end of the pulse, which is equal for both electrons and given by equation 1 (replace t_0 by the rescattering time t_{12}). For each recollision energy this leads to a classically allowed region of phase space, which is a circle centered on the diagonal in figure 12. An example is shown in figure 16.

If the recollision energy is below the field free ionization threshold still double ionization might occur. Any detailed scenario for this case without an explicit calculation is rather speculative since one deals with an excitation process in a very strong field environment for which no experiment exist so far. Already the levels of excited states are strongly modified compared to the field free case. The same will certainly be true for the cross sections. We can however distinguish two extreme cases: An excited intermediate complex is formed, which is either quenched immediately by the field or it may survive at least half a cycle of the field and will be quenched close to the next field maximum. The probability of such survival will depend on the field at the time of the return. For 3.8 or $4.7 \cdot 10^{14} W/cm^2$ the field at times corresponding to a return energy sufficient to reach the first excited states of an Ar^{1+} ion (at about $16 - 17eV$ field free) is so high that such a state would be above the barrier and hence not be bound. A scenario which leads to the observed momentum of a $0.9 - 1au$ for 3.8 and $4.7 \cdot 10^{14} W/cm^2$ (data of figures 12, 13) is the following [17, 43]:

Electron 1 has a return energy of about $17eV$, which corresponds to the first exited states of the Ar^{1+} ion. Electron 1 is stopped, electron 2 is excited and immediately field ionized. Both electrons thus start with momentum zero at the time of the recollision. They are accelerated in the field and, hence, end up with the same momentum of about $0.9 - 1au$ after the pulse. This is in good agreement with the experimental observations for electrons emitted in the same hemisphere. It does not explain, however, a considerable number of events ejected into opposite hemispheres along the laser polarization.

Feuerstein et al performed the same experiment in argon at a lower laser intensity of $2.5{\cdot}10^{14}W/cm^2$ [45] (see figure 17). In this case sufficiently high return energies for excitation correspond to a return time close to the zero crossing of the field. Therefore one can expect that the excited state survives at least till the next field maximum. Feuerstein et al estimated an expected region in phase space for excitation as shown in figure 17. For recollision events where the second electron is lifted into the continuum the allowed region of phase space is somewhat smaller than in figure 16 and confined to the two circles on the diagonal. Feuerstein et al used this argument to separate events in which the recollision leads to an excited state and those which involve electron impact ionization.

Supporting this notion of an intermediate excited complex Peterson and Bucksbaum reported an enhanced production of low energy electrons in the ATI electron spectrum of argon [81] previously unobserved which can be interpreted in terms of inelastic excitation of Ar^+ or of multiple returns of the first electron. Electrons from excited states field ionized at the field maximum will be detected with very little momentum as they receive almost no drift velocity in the laser field.

D. S-matrix calculations

The full diagram shown in figure 8 has not yet been evaluated to obtain the correlated electron momentum distribution. Goreslavskii and Popruzhenko succeeded, however, to calculate those distributions by making use of the saddle point approximation in the integration (see figure 18). The calculations shown in figure 18 are restricted to zero transverse momentum, similar distribution for neon and argon integrated over all transverse momenta can be found in [86]. These calculations do not include intermediate excited states but only the direct (e,2e) process. The calculations do not show a maximum on the diagonal as seen in

the experiments. In contrary they favor the situation where one electron is slow and the other one fast. The authors point out that this is a direct consequence of the sharing of the excess energy in the (e,2e) collision; the long range Coulomb potential favors small momentum transfer in the collision. By replacing the Coulomb potential with a contact potential Goreslavskii and coworkers find a distribution which peaks on the diagonal, much like the experimental results. The main reason is that a contact potential does not emphasize small momentum transfers. It has to remain open at present how well justified such a modification of the interaction potential is.

These calculations have been restricted to electrons with zero transverse momentum. The trend seen in these calculations is in agreement with the observation by Weckenbrock et al shown in figure 13a, where one electron was confined to small transverse momenta. The calculations do not include intermediate excited states but only direct electron impact ionization during rescattering. Therefore the theoretical results are not too surprising since electron impact ionization favors unequal energy sharing at the return energies dominating here. In later work Goreslavskii and coworkers have shown that by introducing a contact potential as an additional approximation instead of the full Coulomb potential the distribution peaks on the diagonal [86]. This is probably due to a modification of the most likely momentum exchange in the electron impact ionization and it has to remain open at present how realistic this is.

E. Time dependent calculations

Calculations by the Taylor group solving the time dependent Schrödinger equation in three dimensions predicted the emission of both electrons to the same side prior to the experimental observation [65]. Similar conclusions have been drawn from one dimensional calculations [102]. In the low field, short wavelength regime the full calculations have proven to be able to predict electron-electron angular distributions and the energy sharing among the electrons as well as the total double ionization cross section [70, 103]. In the strong field case at $800nm$, however, the calculations are extremely demanding. No electron-electron momentum space distributions have been reported up to now. The total double ionization rates however are in good agreement with the observations at $380nm$ [67].

Several one dimensional calculations have been performed at $800nm$. All calculations

show the majority of electrons emitted to the same side [34, 104, 105]. From the calculated electron densities in coordinates space Lein and coworkers have obtained momentum distributions (figure 19). The enhanced emission probability in the first and third quadrant at intermediate in panels (d) and (e) is clearly visible. Different from the experiment, however, a strongly reduced probability is observed along the diagonal, which is most likely an artifact of the one-dimensional model. While in three dimensions electron repulsion can lead to an opening angle between the electrons having the same momentum component in the polarization direction, this is impossible in one dimension. Here the electron repulsion necessarily leads to a node on the diagonal for electrons emitted at the same instant in the field.

For $400nm$ radiation these calculations have also shown clear rings corresponding to ATI peaks in the sum energy of both electrons [106]. Analogous to ATI peaks in single ionization they are spaced by the photon energy. Similar rings have been seen also in three dimensional calculations at shorter wavelength [66].

VIII. OUTLOOK

The application of COLTRIMS yielded the first differential data for double ionization in strong laser fields. Compared to the experimental situation in double ionization by single photon absorption, however, the experiments are still in their infancy. So far correlated electron momenta have been measured only for argon and neon. Clearly experiments on helium are highly desirable since this is where theory is most tractable. Also, mainly the momentum component in the polarization direction has been investigated so far, resulting in a big step forward in the understanding of multiple ionization in strong laser fields. None of the experiments up to now provided fully differential data since not all six momentum components of the two electrons were analyzed. Therefore, no coincident angular distributions as for single photon absorption are available at this point (see [88] for a theoretical prediction of these distributions). Most important for such future studies is a high resolution of the sum energy of the two electrons, which would allow to count the number of photons absorbed. From single photon absorption it is known that angular distributions are prominently governed by selection rules resulting from angular momentum and parity, hence, from the even or oddness of the number of absorbed photons.

Another important future direction is a study of the wavelength dependence of double ionization. The two cases of single and multiphoton absorption discussed here are only the two extremes. The region of two and few photon double ionization is experimentally completely unexplored. Experiments for two photon double ionization of helium will become feasible in the near future at the VUV FEL facilities such as the TESLA Test facility in Hamburg.

ACKNOWLEDGMENTS

The Frankfurt coauthors would like to thank H. Giessen, G. Urbasch, H. Roskos , T. Löffler and M. Thomson for collaboration on some of the experiments described here and C. Freudenberger for preparation of many of the figures. The Heidelberg coauthors are indebted to the Max-Born-Institute in Berlin, providing the laser facilities for the experiments. Moreover, H. Rottke, C. Trump, M. Wittmann, G. Korn and W. Sandner made decisive contributions to the experimental setup, helping in the realization of the experiments during beam-times and contributed strongly in the evaluation and interpretation of the data. We thank A. Becker, F. Faisal and W. Becker for many helpful discussions and for educating us on S-matrix theory. We have also profited tremendously from discussions with K. Taylor, D. Dundas, M. Lein, V. Engel, J. Feagin, L. DiMauro and P. Corkum. This work is supported by DFG, BMBF, GSI. R.D. acknowledges supported by the Heisenberg-Programm of the DFG. R.M., B.F. and J.U. acknowledge support by the Leibniz-Programm of the DFG. T. W. is grateful for financial support of the Graduiertenförderung des Landes Hessen.

REFERENCES

[1] M. Göppert-Mayer, Ann. d. Phys. **9**, 273 (1931).

[2] K. Burnett, V. Reed, and P. Knight, J. Phys **B26**, 561 (1993).

[3] L. DiMauro and P. Agostini, Advances in Atomic and Molecular Physics (Academic Press), New York 1995 (1995).

[4] M. Protopapas, C. Keitel, and P. Knight, Physics Reports **60**, 389 (1997).

[5] S. Backus, C. Durfee, M. Murnane, and H. Kapteyn, Rev. Sci. Instrum. **69**, 1207 (1998).

[6] T. Brabec and F. Krausz, Rev. Mod. Phys. **72**, 545 (2000).

[7] J.-C. Diels and W. Rudolph, *Ultrashort Laser Pulse Phenomena* (Academic Press, 1995).

[8] C. Rulliere, *Femtosecond Laser Pulses. Principles and Experiments* (Springer Verlag, New York, 1998).

[9] R. Dörner, V. Mergel, O. Jagutzki, L. Spielberger, J. Ullrich, R. Moshammer, and H. Schmidt-Böcking, Physics Reports **330**, 96 (2000).

[10] J. McGuire, Electron Correlation Dynamics in Atomic Collisions (Cambridge 1997, Cambridge University Press).

[11] J. McGuire, N. Berrah, R. Bartlett, J. Samson, J. Tanis, C. Cocke, and A. Schlachter, J. Phys. **B28**, 913 (1995).

[12] J. Briggs and V. Schmidt, J. Phys. **33**, R1 (2000).

[13] S. Wolf and H. Helm, Phys. Rev. **A56**, R4385 (1997), .

[14] M. van der Poel, C. V. Nielsen, M.-A. Gearba, and N. Andersen, Phys. Rev. Lett. **87**, 123201 (2001).

[15] J. W. Turkstra, R. Hoekstra, S. Knoop, D. Meyer, R. Morgenstern, and R. E. Olson, Phys. Rev. Lett. **87**, 123202 (2001).

[16] X. Flechard, H. Nguyen, E. Wells, I. Ben-Itzhak, and B. D. DePaola, Phys. Rev. Lett. **87**, 123203 (2001).

[17] T. Weber, H. Giessen, M. Weckenbrock, A. Staudte, L. Spielberger, O. Jagutzki, V. Mergel, G. Urbasch, M. Vollmer, and R. Dörner, Nature **404**, 608 (2000).

[18] R. Moshammer, M. Unverzagt, W. Schmitt, J. Ullrich, and H. Schmidt-Böcking, Nucl. Instr. Meth. **B 108**, 425 (1996).

[19] V. Schyja, T. Lang, and H. Helm, Phys. Rev. **57**, 3692 (1998).

[20] H. Helm, N. Bjerre, M. Dyer, D. Huestis, and M. Saeed, Phys. Rev. Lett **70**, 3221 (1993).

[21] K. Hino, T. Ishihara, F. Shimizu, N. Toshima, and J.H. McGuire, Phys. Rev. **A48**, 1271 (1993).

[22] A. Kheifets, I. Bray, K. Soejima, A. Danjo, K. Okuno, and A. Yagishita, J. Phys. **B34**, L247 (2001).

[23] R. Shingal and C. Lin, J. Phys **B24**, 251 (1991).

[24] P. Lambropoulos, P. Maragakis, and J. Zhang, Physics Reports **305**, 203 (1998).

[25] R. Dörner, H. Bräuning, J. Feagin, V. Mergel, O. Jagutzki, L. Spielberger, T. Vogt, H. Khemliche, M. Prior, J. Ullrich, et al., Phys. Rev. **A57**, 1074 (1998).

[26] F. Byron and C. Joachain, Phys. Rev. **164**, 1 (1967).

[27] L. Spielberger, O. Jagutzki, R. Dörner, J. Ullrich, U. Meyer, V. Mergel, M. Unverzagt, M. Damrau, T. Vogt, I. Ali, et al., Phys. Rev. Lett. **74**, 4615 (1995).

[28] L. Spielberger, H. Bräuning, A. Muthig, J. Tang, J. Wang, Y. Qui, R. Dörner, O. Jagutzki, T. Tschentscher, V. Honkimäki, et al., Phys. Rev. **59**, 371 (1999).

[29] J. Samson, Phys. Rev. Lett. **65**, 2863 (1990).

[30] M. Y. Kuchiev, Sov. Phys.-JETP Lett. **45**, 404 (1987).

[31] P. Corkum, Phys. Rev. Lett. **71**, 1994 (1993).

[32] K. Schafer, B. Yang, L. DiMauro, and K. Kulander, Phys. Rev. Lett. **70**, 1599 (1993).

[33] J. Watson, A. Sanpera, D. Lappas, P. Knight, and K. Burnett, Phys. Rev. Lett. **78**, 1884 (1997).

[34] M. Lein, E. Gross, and V. Engel, Phys. Rev. Lett. **85**, 4707 (2000).

[35] M. Lein, E. Gross, and V. Engel, Optics Express **8**, 441, http://www.opticsexpress.org/oearchive/source/30744.htm (2001).

[36] D. Fittinghoff, P. Bolton, B. Chang, and K. Kulander, Phys. Rev. **A49**, 2174 (1994).

[37] P. Dietrich, N. H. Burnett, M. Ivanov, and P. B. Corkum, Phys. Rev. **A50**, R3585 (1994).

[38] B. Witzel, N. A. Papadogiannis, and D. Charalambidis, Phys. Rev. Lett. **85**, 2268 (2000).

[39] R. Lafon, J. L. Chaloupka, B. Sheehy, P. M. Paul, P. Agostini, K.C.Kulander, , and L. F. DiMauro, Phys. Rev. Lett. **86**, 2762 (2001).

[40] T. Weber, M. Weckenbrock, A. Staudte, L. Spielberger, O. Jagutzki, V. Mergel, G. Urbasch, M. Vollmer, H. Giessen, and R. Dörner, Phys. Rev. Lett. **84**, 443 (2000).

[41] R. Moshammer, B. Feuerstein, W. Schmitt, A. Dorn, C. Schröter, J. Ullrich, H. Rottke, C. Trump, M. Wittmann, G. Korn, et al., Phys. Rev. Lett. **84**, 447 (2000).

[42] T. Weber, O. Jagutzki, M. Hattass, A. Staudte, A. Nauert, L. Schmidt, M. Prior, A. Landers, A. Bräuning-Demian, H. Bräuning, et al., J. Phys. **B34**, 3669 (2001).

[43] M. Weckenbrock, M. Hattass, A. Czasch, O. Jagutzki, L. Schmidt, T. Weber, H. Roskos, T. Löffler, M. Thomson, and R. Dörner, J. Phys **B34**, L449 (2001).

[44] M. Weckenbrock, Diploma Thesis (J.W. Goethe University Frankfurt/Main, 2001).

[45] B. Feuerstein, R. Moshammer, D. Fischer, A. Dorn, C. D. Schröter, J. Deipenwisch, J. Lopez-Urrutia, C. Höhr, P. Neumayer, J. Ullrich, et al., Phys. Rev. Lett. **87**, 043003 (2001).

[46] T. Weber, M. Weckenbrock, A. Staudte, L. Spielberger, O. Jagutzki, V. Mergel, G. Urbasch, M. Vollmer, H. Giessen, and R. Dörner, J. Phys **B33**(L127) (2000).

[47] S. Larochelle, A. Talebpour, and S. L. Chin, J. Phys **B31**, 1201 (1998).

[48] R. M. et al, Phys. Rev. Lett. , submitted for publication (2001).

[49] N. Delone and V. Krainov, Physics Uspeki **41**, 469 (1998).

[50] B. Feuerstein, R. Moshammer, and J. Ullrich, J. Phys **B33**, L823 (2000).

[51] A. Becker and F. Faisal, Phys. Rev. Lett. **84**, 3546 (2000).

[52] A. Becker and F. Faisal, J. Phys **B29**, L197 (1996).

[53] A. Becker and F. Faisal, Phys. Rev. **A59**, R1742 (1999).

[54] A. Becker and F. Faisal, J. Phys **B32**, L335 (1999).

[55] V. R. Bhardwaj, S. A. Aseyev, M. Mehendale, G. L. Yudin, D. M. Villeneuve, D. M. Rayner, M. Y. Ivanov, and P. B. Corkum, Phys. Rev. Lett. **86**, 3522 (2001).

[56] R. Kopold, W. Becker, H. Rottke, and W. Sandner, Phys. Rev. Lett. **85**, 3781 (2000).

[57] S. Goreslavskii and S. Popruzhenko, Optics Express **8**, 395, http://www.opticsexpress.org/oearchive/source/30694.htm (2001).

[58] S. Goreslavskii and S. Popruzhenko, J. Phys **B34**, L239 (2001).

[59] J. Chen, J. Liu, L. Fu, and W. Zheng, Phys. Rev. **63**, 011404R (2000).

[60] K. Sacha and B. Eckhardt, Phys. Rev. **63**, 043414 (2001).

[61] J. Feagin, J. Phys. **B28**, 1495 (1995).

[62] J. Feagin, J. Phys. **B29**, l551 (1996).

[63] R. Dörner, J. Feagin, C. Cocke, H. Bräuning, O. Jagutzki, M. Jung, E. Kanter, H. Khemliche, S. Kravis, V. Mergel, et al., Phys. Rev. Lett. **77**, 1024 (1996), see also erratum in Phys. Rev. Lett. 78. 2031 (1997).

[64] K. Sacha and B. Eckhardt, Phys. Rev. **64**, 053401 (2001).

[65] K. Taylor, J. Parker, D. Dundas, E. Smyth, and S. Vitirito, Laser Physics **9**, 98 (1999).

[66] J. S. Parker, L. R. Moore, K. J. Meharg, D. Dundas, and K. T. Taylor, J. Phys **B34**, L69 (2001).

[67] J. S. Parker, L. R. Moore, D. Dundas, and K. T. Taylor, J. Phys **B33**, L691 (2000).

[68] J. Parker, K. Taylor, C. Clark, and S. Blodgett-Ford, J. Phys **B29**, L33 (1996).

[69] D. Dundas, K. Taylor, J. Parker, and E. Smyth, J. Phys **B32**, L231 (1999).

[70] J. Colgan, M. S. Pindzola, and F. Robicheaux, J. Phys. **34**, L457 (2001).

[71] K. LaGattuta and J. Cohen, J. Phys **B31**, 5281 (1998).

[72] C. Feeler and R. Olson, J. Phys. **33**, 1997 (2000).

[73] A. Cassimi, S. Duponchel, X. Flechard, P. Jardin, P. Sortais, D. Hennecart, and R. Olson, Phys. Rev. Lett. **76**, 3679 (1996).

[74] R. Dörner, J. Ullrich, H. Schmidt-Böcking, and R. Olson, Phys. Rev. Lett. **63**, 147 (1989).

[75] R. Dörner, V. Mergel, R. Ali, U. Buck, C. Cocke, K. Froschauer, O. Jagutzki, S. Lencinas, W. Meyerhof, S. Nüttgens, et al., Phys. Rev. Lett. **72**, 3166 (1994).

[76] R. Dörner, H. Khemliche, M. Prior, C. Cocke, J. Gary, R. Olson, V. Mergel, J. Ullrich, and H. Schmidt-Böcking, Phys. Rev. Lett. **77**, 4520 (1996).

[77] V. Frohne, S. Cheng, R. Ali, M. Raphaelian, C. Cocke, and R. Olson, Phys. Rev. Lett. **71**, 696 (1993).

[78] V. Mergel, R. Dörner, M. Achler, K. Khayyat, S. Lencinas, J. Euler, O. Jagutzki, S. Nüttgens, M. Unverzagt, L. Spielberger, et al., Phys. Rev. Lett. **79**, 387 (1997).

[79] R. Moshammer, J. Ullrich, M. Unverzagt, W. Schmidt, P. Jardin, R. Olson, R. Mann, R. Dörner, V. Mergel, U. Buck, et al., Phys. Rev. Lett. **73**, 3371 (1994).

[80] R. Moshammer, J. Ullrich, H. Kollmus, W. Schmitt, M. Unverzagt, O. Jagutzki, V. Mergel, H. Schmidt-Böcking, R. Mann, C. Woods, et al., Phys. Rev. Lett. **77**, 1242 (1996).

[81] E. Peterson and P. Bucksbaum, Phys. Rev. **64**, 053405 (2001).

[82] R. Moshammer, B. Feuerstein, D. Fischer, A. Dorn, C. Schröter, J. Deipenwisch, J. Lopez-Urrutia, C. Höhr, P. Neumayer, J. Ullrich, et al., Optics Express **8**, 358, http://www.opticsexpress.org/oearchive/source/30944.htm (2001).

[83] V.Mergel, M. Achler, R. Dörner, K. Khayyat, T. Kambara, Y. Awaya, V. Zoran, B. Nyström, L.Spielberger, J. McGuire, et al., Phys. Rev. Lett. **80**, 5301 (1998).

[84] M. Achler, V. Mergel, L. Spielberger, Y. A. R. Dörner, and H. Schmidt-Böcking, J. Phys. **B34**, L965 (2001).

[85] R. Moshammer, B. Feuerstein, I. C. L. Urrutin, A. Dorn, D. Fischer, C. Schröter, W. Schmitt, J. Ullrich, H. Rottke, C. Trump, et al., Phys. Rev. (submitted).

[86] S. Goreslavskii, S. Popruzhenko, R. Kopold, and W. Becker, Phys. Rev. **64**, 053402

(2001).

[87] T. Weber, M. Weckenbrock, A. Staudte, M. Hattass, L. Spielberger, O. Jagutzki, V. Mergel, G. U. H. Schmidt-Böcking, H. Giessen, H. Bräuning, et al., Optics Express **7**(9), 368, http://www.opticsexpress.org/oearchive/source/30623.htm (2001).

[88] A. Becker and F. Faisal, Phys. Rev. **A50**, 3256 (1994).

[89] R. Dörner, V. Mergel, H. Bräuning, M. Achler, T. Weber, K. Khayyat, O. Jagutzki, L. Spielberger, J. Ullrich, R. Moshammer, et al., Atomic processes in Plasmas **AIP conference proceedings 443 (1998)** (1998), ed.: E. Oks, M. Pindzola.

[90] A. Dorn, R. Moshammer, C. Schröter, T. Zouros, W. Schmitt, H. Kollmus, R. Mann, and J. Ullrich, Phys. Rev. Lett **82**, 2496 (1999).

[91] A. Dorn, A. Kheifets, C. D. Schröter, B. Najjari, C. Höhr, R. Moshammer, and J. Ullrich, Phys. Rev. Lett **86**, 3755 (2001).

[92] I. Taouil, A. Lahmam-Bennani, A. Duguet, A. Duguet, and L. Avaldi, Phys. Rev. Lett **81**, 4600 (1998).

[93] B. Bapat, S. Keller, R. Moshammer, R. Mann, and J. Ullrich, J. Phys **B33**, 1437 (2000).

[94] R. Moshammer, J. Ullrich, W. Schmitt, H. Kollmus, A. Cassimi, R. Dörner, R. Dreizler, O. Jagutzki, S. Keller, H.-J. Lüdde, et al., Phys. Rev. Lett. **79**, 3621 (1997).

[95] C. von Weizäcker, Zeitschrift für Physik **88**, 612 (1934).

[96] E. Williams, Phys. Rev. **45**, 729 (1934).

[97] S. Keller, H. Lüdde, and R. Dreizler, Phys. Rev. **A55**, 4215 (1997).

[98] A. Voitkiv and J. Ullrich, J. Phys **43**, 1673 (2001).

[99] S. Keller, J. Phys. **B33**, L513 (2000).

[100] M. Unverzagt, R. Moshammer, W. Schmitt, R. Olson, P. Jardin, V. Mergel, J. Ullrich, and H. Schmidt-Böcking, Phys. Rev. Lett. **76**, 1043 (1996), .

[101] M. C. et al., Rev.Mod.Phys. **66**, 985 (1994, and References therein).

[102] M. Lein, E. Gross, and V. Engel, J. Phys **B33**, 433 (2000).

[103] M. Pindzola and F. Robicheaux, Phys. Rev. **A57**, 318 (1998).

[104] S. L. Haan, N. Hoekema, S. Poniatowski, W.-C. Liu, and J. H. Eberly, Optics Express **7**, 29, http://www.opticsexpress.org/oearchive/21863.htm (2000).

[105] H. Muller, Optics Express **8**, 417,
http://www.opticsexpress.org/oearchive/source/30932.htm (2001).

[106] M. Lein, E. Gross, and V. Engel, Phys. Rev. **A64**, 023406 (2001).

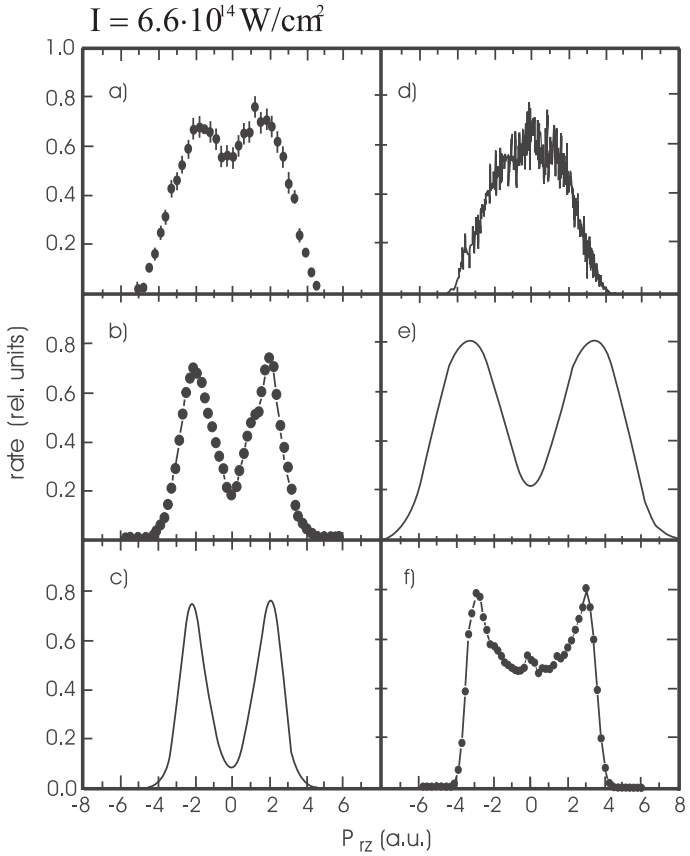

FIG. 9: Momentum distribution of He^{2+} ions at an intensity of $6.6 \cdot 10^{14} W/cm^2$ for all panels. p_{rz} is the component parallel to the laser polarization. a) experiment (from [40]), b) results of the S-matrix calculation (from Becker and Faisal [51]), c) S-matrix with additional saddle point approximation (from Goreslavskii and Popruzhenko [57]), d) solution of the one dimensional Schrödinger equation (from Lein et al. [34]), e) Classical Trajectory Monte Carlo calculations (from Chen et al. [59]) and f) Wannier type calculation (from Sacha and Eckhardt [60]).

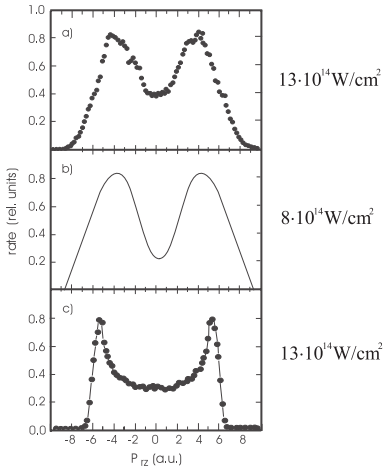

FIG. 10: Momentum distribution of Ne^{2+}. a) projection of data in figure 6(2) at $13 \cdot 10^{14} W/cm^2$ (from Moshammer et al [41]), b) S-matrix calculation evaluating the diagram in figure 8 with contact potentials at $8 \cdot 10^{14} W/cm^2$ (from Kopold et al [56]) and c) Wannier-type calculation at $13 \cdot 10^{14} W/cm^2$ (from Sacha and Eckhardt [60]).

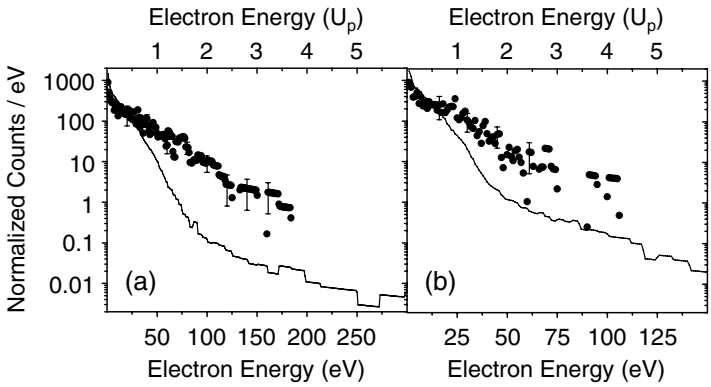

FIG. 11: Electron energy spectra from single ionization (full line) and double ionization (dots) of helium at (a) $8 \cdot 10^{14} W/cm^2$ and (b) $4 \cdot 10^{14} W/cm^2$ (from [39])

.

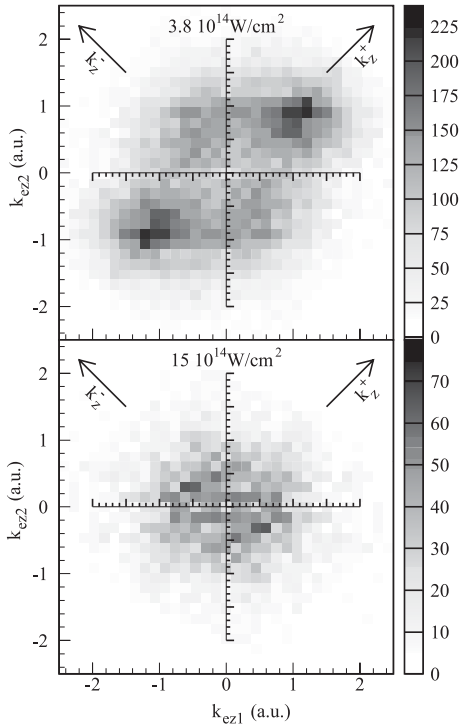

FIG. 12: Momentum correlation between the two emitted electrons when an Ar^{2+} ion is produced in the focus of a $220fs$, $800nm$ laser pulse at peak intensities of $3.8 \cdot 10^{14} W/cm^2$ and $15 \cdot 10^{14} W/cm^2$. The horizontal axis shows the momentum component of one electron along the polarization of the laser field; the vertical axis represents the same momentum component of the corresponding second electron. Same sign of the momenta for both electrons represents an emission to the same half sphere. The data are integrated over the momentum components in the direction perpendicular to the polarization direction. The gray shading shows the differential rate in arbitrary units on a linear scale (adapted from [17]). Compare also figure to 17.

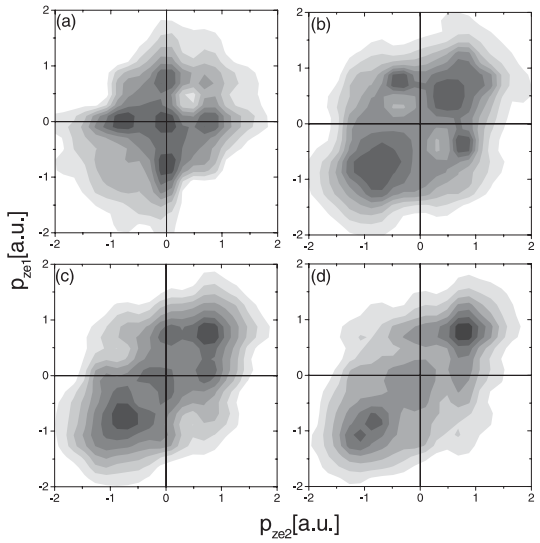

FIG. 13: Momentum correlation between the two emitted electrons when an Ar^{2+} ion is produced in the focus of a $150fs$, $780nm$ laser pulse at peak intensities of $4.7 \cdot 10^{14} W/cm^2$. Axis as in figure 12. Each panel panel represents a part of the final state for a fixed transverse momentum ($p_\perp$) of one of the electrons. (a) One of the electrons has a transverse momentum of $p_\perp < 0.1au$, (b) $0.1 < p_\perp < 0.2au$, (c) $0.2 < p_\perp < 0.3au$, (d) $0.3 < p_\perp < 0.4au$. The gray scale shows the differential rate in arbitrary units and linear scale (from [43]).

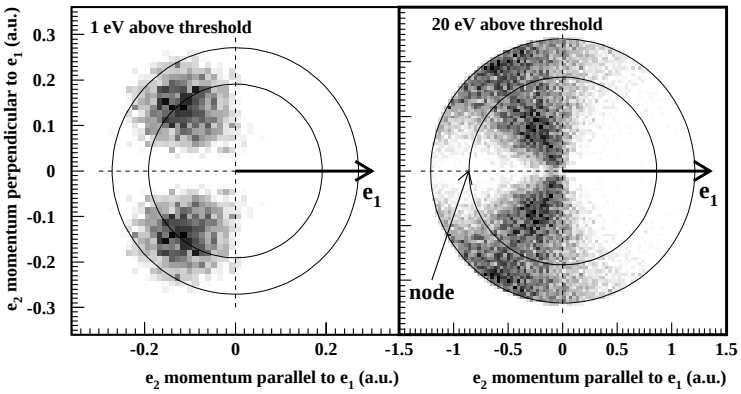

FIG. 14: Single-photon double ionization of He at $1eV$ and $20eV$ above threshold by linearly polarized light (synchrotron radiation). Shown is the momentum distribution of electron 2 for fixed direction of electron 1 as indicated. The plane of the figure is the internal momentum plane of the two particles. The data are integrated over all orientations of the polarization axis with respect to this plane. The figure thus samples the full cross section and all angular and energy distributions of the fragments. The outer circle corresponds to the maximum possible electron momentum; the inner one represents the case of equal energy sharing (from [89] compare also [84]).

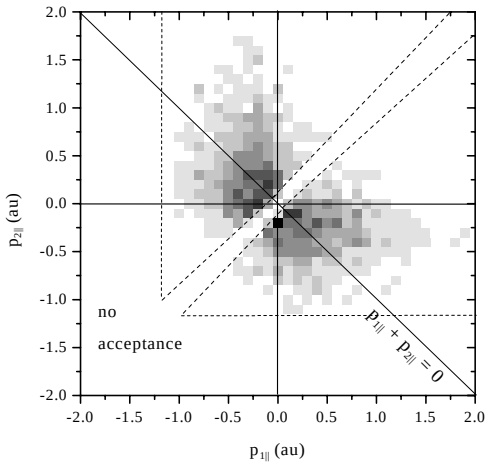

FIG. 15: Double ionization of helium by $100MeV/u$ C^{6+} impact. The horizontal and vertical axis ($p_{1\|}$ and $p_{2\|}$) shows the momentum component of electron 1 and 2 parallel to the direction of the projectile. The dashed curves demarcate the region of the two-eletron momentum space which is not accessed by the spectrometer. The gray scale is linear (adapted from [93]).

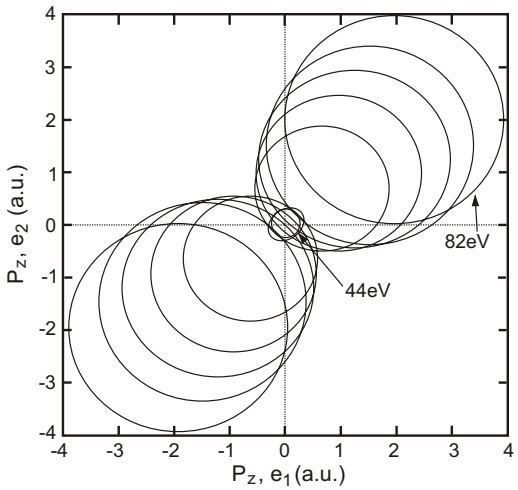

FIG. 16: Classically allowed region of phase space within the rescattering model for double ionization of argon by $4.7 \cdot 10^{14} W/cm^2$, $800nm$ light. Each circle corresponds to a fixed recollision energy. Axis as in figure 12 (adapted from [44]).

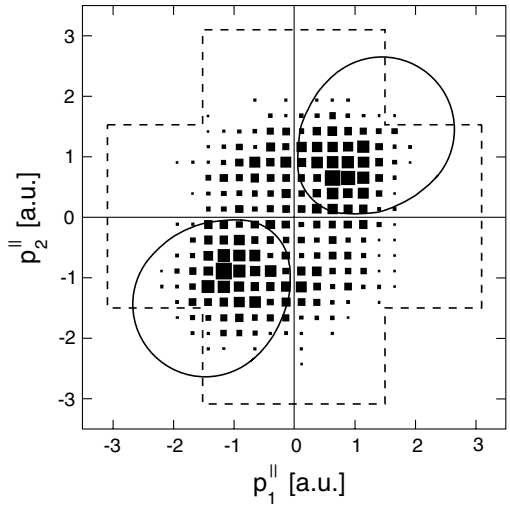

FIG. 17: Correlated electron momentum spectrum of two electrons emitted from argon atoms at $0.25 \cdot 10^{15W}/cm^2$. $p_1^{\parallel}$ is the electron momentum component along the light polarization axis of electron 1. Dashed line: kinematical constraints for recollision with excitation, assuming the excited state is not immediately quenched. Solid line: kinematical constraints for recollision with (e,2e) ionization (from [45]).

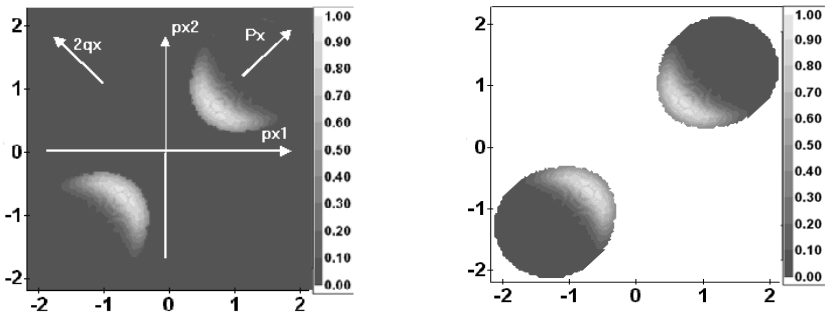

FIG. 18: Two-electron momentum distributions for double ionization of argon (similar to figure 12) calculated evaluating the diagram 8 in the saddle point approximation at an intensity of $3.8{\cdot}10^{14} W/cm^2$. Contrary to the experiment the calculations are not integrated over all momentum components transverse to the field but restricted to electrons with no transverse momentum. The right panel presents the same distribution with the classically forbidden region of phase space shown in white (compare figure 16) (adapted from [57]).

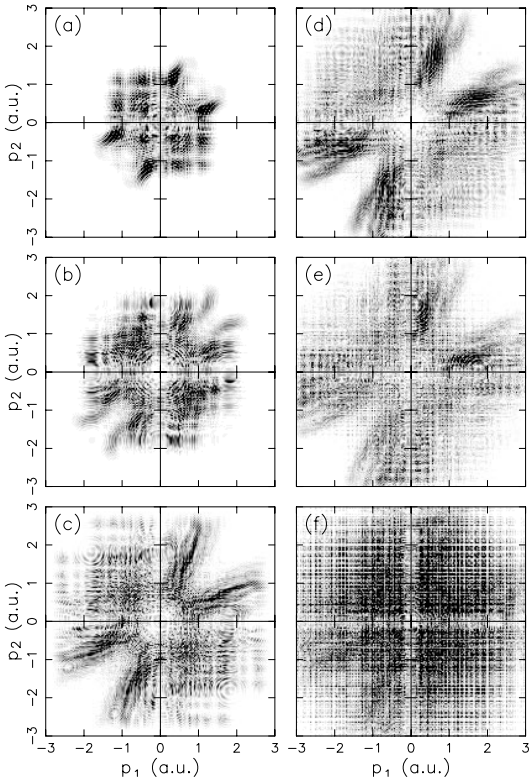

FIG. 19: Two-electron momentum distributions for double ionization of helium (similar to 12) calculated by solving the one dimensional time dependent Schrödinger equation at the intensities of (a) $1{\cdot}10^{14}W/cm^2$, (b) $3{\cdot}10^{14}W/cm^2$, (c) $6.6{\cdot}10^{14}W/cm^2$, (d) $10{\cdot}10^{14}W/cm^2$, (e) $13{\cdot}10^{14}W/cm^2$, (f) $20 \cdot 10^{14}W/cm^2$ (adapted from [34]).